GeoVirtual 2020 September 14-16 Resilience and Innovation

Effect of TBM tunneling in sandy soils on twist behavior of an existing raft foundation

Sumi Siddiqua & Ahmed ElMouchi
Department of Civil Engineering – University of British Columbia, Kelowna, British Columbia, Canada
Asmaa M. Hassan & Mohamed I. Amer
Department of Public Works – Faculty of Engineering - Cairo University, Giza, Egypt

ABSTRACT
Constructing new underground tunnels is a necessity in urban areas to resolve traffic congestion problems. The new tunnels may pass underneath or nearby existing buildings; therefore, the structural safety of the foundations of these buildings should be evaluated. This study focuses on the effect of the TBM tunnel advancement on the twist deformation of an existing raft foundation. The 3D nature of the TBM construction process has been simulated using PLAXIS 3D software. In order to validate the results of the numerical simulation, the resulted settlement trough has been compared to the measured field settlement trough of a selected case study (Second Heinenoord Tunnel in the Netherlands). In the current study, an extensive 3D parametric study is conducted to check the effect of related parameters on the raft twist deformation. The studied parameters include; tunnel cover (Z), skew angle between raft and tunnel (i), raft thickness (d), and raft weight (w).

RÉSUMÉ
La construction de nouveaux tunnels souterrains est une nécessité dans les zones urbaines pour résoudre les problèmes de congestion du trafic dans ces zones. Les nouveaux tunnels passent sous les bâtiments existants, qui pourraient reposer sur une fondation de radeau. Cette étude se concentre sur l'effet de l'avancement du tunnel TBM sur le comportement de torsion de la fondation de radeau existante. La nature 3D du processus de construction TBM a été simulée à l'aide du logiciel PLAXIS 3D. Afin de valider les résultats de la simulation numérique, le creux de tassement résultant a été comparé au creux de tassement mesuré sur le terrain d'une étude de cas sélectionnée (Second tunnel de Heinenoord). Dans la présente étude, une étude paramétrique 3D approfondie est menée pour vérifier l'effet des paramètres connexes sur la torsion du radeau. Les paramètres étudiés comprennent ; couverture du tunnel (Z), inclinaison du radeau (i), épaisseur du radeau (d) et poids du radeau. Les résultats ont révélé que la torsion du radeau est grandement affectée par la couverture du tunnel (Z), l'inclinaison du radeau (i) et l'épaisseur du radeau (d). Cependant, le poids du radeau n'affecte pas le comportement de torsion du radeau.

1 INTRODUCTION

The increasing number of populations in big cities is pushing the transportation sectors to move toward constructing underground transportations systems. These systems help to avoid the problems arising from the above-ground traffic congestions. According to Bernat and Cambou (1998) and Liu et al. (2008), the design and monitoring of underground structures are considered the most crucial challenge for civil engineers. The reason for this is not only the difficulty in designing the underground tunnels but also the influence of the tunneling process on existing structures (Dimmock and Mair, 2008; Pickhavar et al., 2010; Elmouchi et al., 2017).

Mroueh and Shahrour (2003) showed that the analysis of the tunnel-structure interaction is complicated due to the 3D nature of the problem. In the engineering applications, the process of evaluating the effect of underground tunnels on an existing structure is typically conducted in two steps. The first step is to determine the ground settlement due to the construction of the tunnel by empirical methods (Peck, 1969), analytical methods (Sagasta, 1987; Verruijt and Booker, 1996), or numerical methods (González and Sagaset, 2001; Moller, 2006). The second step is to check the suitability of the structure to sustain these new movements and stresses. This approach ignores the 3D nature of the problem, the interaction between tunnel and structure and the structure stiffness, which are proven to be significant (Mroueh and Shahrour, 2003; Burd et al., 2000; Keshuan and Lieyun, 2008; Elmouchi et al., 2018, Siddiqua, et al., 2018).

One of the consequences of constructing tunnels underneath an existing raft foundation is the raft twist deformation. This term has been introduced by Franzius et al. (2006). The raft twist deformation is a function of the

differential settlement of the raft corners, as stated in equation (1).

$$\theta = \frac{\frac{S_{v,a}-S_{v,b}}{L} - \frac{S_{v,c}-S_{v,d}}{L}}{B} \text{ (1/unit length)} \quad [1]$$

Where $S_{v,a}$, $S_{v,b}$, $S_{v,c}$, and $S_{v,d}$ are the vertical settlements of the four corners, B and L are the width and the length of the building, respectively. θ is raft twist deformation (1/unit length). Figure 1 shows the geometrical representation of all the previous terms. The positive value of raft twist deformation indicates an increase in the rotation towards the side of the tunnel.

Franzius et al. (2006) concluded that if a new tunnel passes underneath an existing raft, there are two possible types of twist deformations: temporary and permanent. The temporary twist deformation occurs when the existing raft and the new tunnel are perpendicular to each other. In this case, the raft undergoes a temporary twist during the tunnel construction process. As soon as the tunnel moves away from the raft, this temporary twist deformation decreases or even vanishes. The permanent twist deformation occurs when there is a skew angle between the existing raft and the new tunnel. In this case, the existing raft suffers a permanent twist, which is a non-recoverable deformation even after the completion of the tunnel construction.

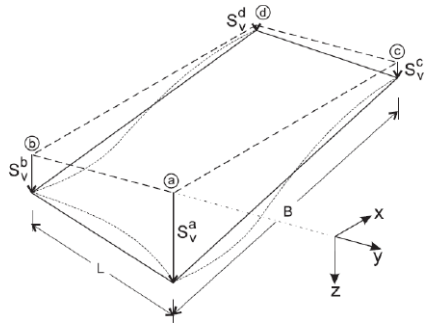

Figure 1. Geometrical representation of different terms in the definition of the raft twist (after Franzius et al., 2006).

This paper aims to study the effect of different geometrical and structural parameters on the induced raft twist deformation when a new tunnel passes underneath. This paper is divided into three sections. The first section demonstrates the numerical simulation of the Second Heinenoord Tunnel as a case study and compares the results of the numerical simulation to the field measurements and the numerical analysis of Moller (2006). The second section presents the geometry of the raft foundation and the properties of the sandy soils. The third part shows the results of the sensitivity analysis. The effects of the tunnel cover (Z), the skew angle between raft and tunnel (i), the raft thickness (d), and the raft weight (w) on the induced raft twist deformation are investigated.

2 CASE STUDY AND NUMERICAL MODEL VALIDATION

Second Heinenoord Tunnel (1998) in the Netherlands is the selected case study based on Moller's (2006) work. This case study has been chosen as it includes field measurements for the surface settlement trough during and after the tunnel construction as well as the numerical simulation of the TBM tunneling process using PLAXIS 3D ©, which is adopted in this study.

The tunnel is a slurry shield TBM type. The soil cover above the tunnel crown is Z = 12.5 m, and the tunnel diameter is D = 8 m. Shell elements as a linear elastic material have been used to simulate the tunnel lining with the following properties: flexural rigidity EI = 26.78 MN.m^2, normal stiffness EA = 10.5 x 10^3 MN, weight w = 24 kN/m^2, and Poisson's ratio υ = 0.15.

The TBM shield is simulated as a radial pressure = 125 kPa. The slurry pressure at the face of the tunnel is applied as an axial pressure = 230 kPa. The grouting at the tail void behind the shield is simulated as a radial pressure = 125 kPa. To account for the increasing overburden pressure with depth, these three pressures are assigned to increase linearly with depth by 15 kPa/m. To simulate the ground-lining gap, ground elements of 20 cm thickness have been deactivated at the tail of the shield. This gap is filled with a hardening grouting material which has the same properties of the lining in the subsequent construction phases. The TBM length is 7.5 m. The pressurized grouting at the TBM tail is 3.0 m long. The total tunnel length is divided into 1.5 m segments to simulate the tunnel advancement process. The total length of the tunnel is 45 m. This length is selected to ensure the steady-state condition of the calculated surface settlement troughs.

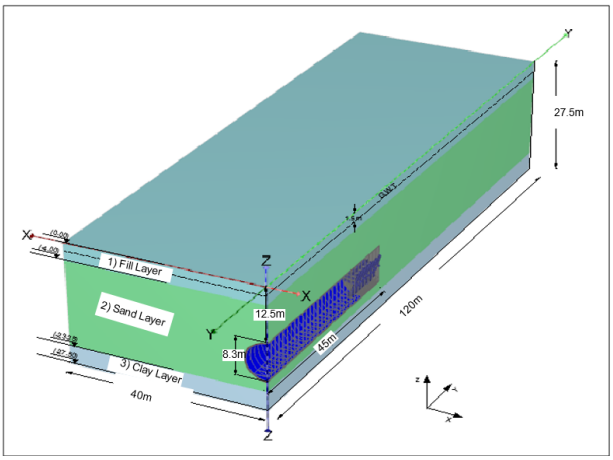

Figure 2. 3D geometry of the Second Heinenoord Tunnel after Moller (2006).

The soil profile at the location of the Second Heinenoord Tunnel is shown in Figure 2. The soil mass is simulated as a continuum divided into several volume elements. The 10-node tetrahedron elements demonstrate the primary soil elements of a 3D finite element mesh. The

various parameters of the different soil layers are presented in Table 1. The groundwater table GWT is encountered at 1.5 m depth below the ground surface.

The generated settlement troughs in transversal and longitudinal directions are calculated from the 3D model along the tunnel advance length. Afterward, they are compared to the settlement trough measured in the field during the construction of the Second Heinenoord tunnel in addition to the results of the numerical simulation of Moller (2006).

Figure 3 shows a good agreement between the field measurements, and the 3D model results from the current study. The calculated maximum settlement is 25 mm, and the longitudinal trough width is about 60 m, which matches the measured values and the numerical simulation of Moller (2006). The calculated settlement curves are flatter than the measured ones. The steepness of the settlement curve is dependent on the soil's constitutive model. In the current study, the hardening soil model is used, which provides a flatter curve (Moller 2006).

Table 1. Soil properties of the 3D model of the Second Heinenoord Tunnel (after Moller, 2006).

Layer	(1) Fill	(2) Sand	(3) Clay
Layer Depth	0 – 4	4 – 23.5	23.5 – 27.5
Saturated unit weight, γ (kN/m^3)	17.2	20	20
Tangent stiffness for the primary oedometer loading, E^{ref}_{oed} (MPa)	14	35	7
Secant stiffness in the standard drained triaxial test, E^{ref}_{50} (MPa)	14	35	12
Unloading/Reloading stiffness, E^{ref}_{ur} (MPa)	42	105	35
Power for the stress-level dependency of stiffness, m	0.5	0.5	0.9
Effective angle of shearing resistance, ϕ' (deg.)	27	35	31
Effective cohesion, c' (kPa)	3	0.01	7
At rest Earth pressure coefficient, K_o	0.58	0.47	0.55
Poisson's ratio, υ_{ur}	0.2	0.2	0.2

3 RAFT CONFIGURATION AND STAGES OF CONSTRUCTION

The raft dimensions are 20 m length, 20 m width, and 1 m thickness. The spacing between columns equals 4.5 m. The distance between the external columns and the raft edge is 1 m. The column loads have been applied such that

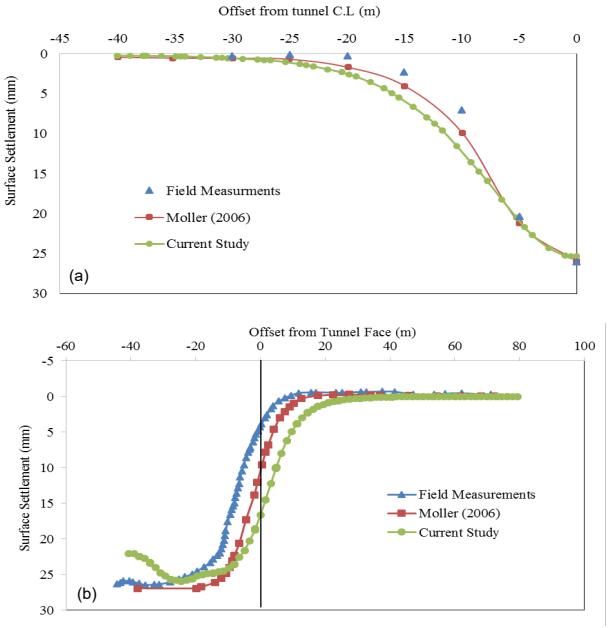

Figure 3. comparison of surface settlement troughs along the: (a) transversal direction, (b) longitudinal direction.

the average stress underneath the raft equals 100 kPa. The raft has been simulated as a plate element of linear elastic concrete properties of young's modulus E = 2 x 10^7 kN/m^2 and Poisson's ratio υ = 0.15. Medium dense sand has been simulated using the Hardening Soil Model (Table 2). The 3D geometrical configuration of the raft and the tunnel is shown in Figure 4. It should be noted that the model dimensions are selected such that the borders of the model have no effect either on the raft settlements or on the induced settlement troughs due to the tunneling process.

Table 2. Hardening soil model properties of medium dense sandy soils.

Soil Type	Medium Dense Sand
Unsaturated unit weight, γ_{unsat}(kN/m^3)	16
Saturated unit weight, γ_{sat} (kN/m^3)	18
Tangent stiffness for primary oedometer loading, E^{ref}_{oed} (MPa)	35
Secant stiffness in the standard drained triaxial test, E^{ref}_{50} (MPa)	35
Unloading/Reloading stiffness, E^{ref}_{ur} (MPa)	105
Power for the stress-level dependency of stiffness, m	0.5
Effective angle of shearing resistance, ϕ (deg.)	35
Effective cohesion, c' (kPa)	0.01
At rest Earth pressure coefficient, K_o	0.426
Poisson's ratio, υ_{ur}	0.25

The construction stages of the tunnel have been considered in the simulation to check the effect of the tunnel advancement on the raft twist deformation. Soil's initial stresses are generated using the K_0 procedure in the first stage. In the second stage, the raft volume element and loads are activated. For the third stage, the TBM face and shield are activated along the first segment of the tunnel, and the soil element within this segment is deactivated. In the fourth stage, as the tunnel advances, TBM face and shield are activated along the next segment, and soil element within this segment is deactivated. Meanwhile, the shield in the previous segment is replaced by the tunnel lining. The same procedure of the fourth stage is repeated until reaching the end of tunnel length.

4 SENSITIVITY ANALYSIS

The effects of tunnel cover (Z), skew angle between raft and tunnel (i), raft thickness (d), and raft weight (w) on the raft twist deformation are presented in this section. For the reference case, the tunnel diameter (D) = 8 m, the tunnel cover (Z) = 12 m, the horizontal clearance (CL) = zero, the skew angle between raft and tunnel (i) = zero, and raft thickness (d) = 1 m.

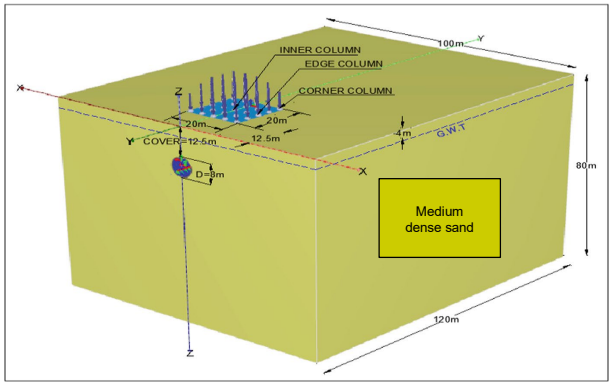

Figure 4. Raft and tunnel geometrical interaction and model boundaries.

4.1 Effect of tunnel cover (Z)

Four finite element models have been used to investigate the effect of the tunnel cover (Z) on the raft twist deformation (θ). The Greenfield case is studied in two models in which the twist deformation is calculated at the ground surface at the same prescribed location of the raft corners. The tunnel cover values of 12 m (1.5 times the tunnel diameter) and 24 m (3 times the tunnel diameter) are used. The other two models account for the presence of the raft foundation. In the four models, the raft and the tunnel are perpendicular to each other (i = zero).

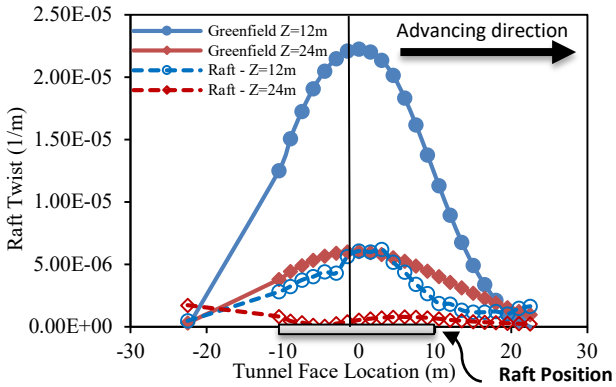

Figure 5. Effect of tunnel cover (Z) on raft twist (θ).

Figure 5 presents the raft twist deformation during the tunnel advancement towards the raft. As the tunnel advances, the raft twist deformation increases and reaches its peak value when the tunnel face is directly beneath the raft centerline, and then the twist decreases again and may vanish at a distance of 20 m from the raft centerline (2.5D). The same trend is observed for both the Greenfield and the raft, which is similar to the findings of Franzius et al. (2006). It is also depicted that the deeper the tunnel, the smaller the raft twist deformation. This could be attributed to the decrease in the ground surface settlement due to the soil arching mechanism as the tunnel cover increases. The maximum raft twist decreases by around 75% in the presence of the raft foundation for the tunnel cover Z = 12 m and by around 80% for the tunnel cover Z = 24 m. The drastic decrease in the raft twist deformation reflects the importance of considering the complicated tunnel-raft interaction in the analysis.

4.2 Effect of skew angle between raft and tunnel (i)

The effect of the skew angle between raft and tunnel (i) on the raft twist deformation (θ) has been studied using three values of i (0°,10°, and 45°). As shown in Figure 6, for the Greenfield case, at small skew angles (i = 0° and 10°), the raft twist follows the same trend. As the tunnel advances, the twist value increases and reaches its peak value when the tunnel face is directly beneath the centerline of the raft, and then the calculated twist decreases as the tunnel advances. However, for a more considerable skew angle value (i = 45°), a temporary peak of raft twist deformation is observed when the tunnel face is directly underneath the raft centerline. Then, the raft twist deformation decreases till the tunnel face is directly below the raft edge. Afterward, the raft twist deformation rises again as the tunnel face advances resulting in a permanent value of twist.

The same trend was confirmed by Franzius et al. (2006) using the equivalent beam model. It should be noted that, for large skew angles, the permanent raft twist deformation is larger than the temporary one. Moreover, at the presence of the raft foundation, the permanent values of raft twist deformations occur also at i = 10°.

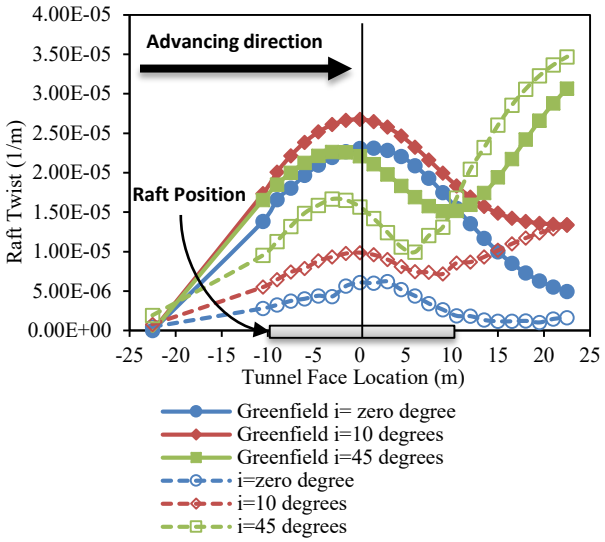

Figure 6. Influence of raft inclination (i) on raft twist (Θ).

4.3 Effect of raft thickness (d)

Investigating the effect of the raft thickness is conducted using five 3D FE models. One model is related to Greenfield. The other four models are conducted in the presence of the raft foundation with four different thicknesses (d = 0.75 m, d = 1.00 m, d = 1.50 m, and d = 2.00 m).

Figure 7 reveals that as the raft thickness increases, smaller values of twist deformations are induced. This could be attributed to the increase in the raft stiffness. Hence, the settlements of the raft corners decrease. Consequently, smaller values of raft twist deformations are obtained. The calculated maximum temporary raft twist when the tunnel face is directly beneath the raft centerline for the green field is 2.3 x 10^{-5} (1/m), but for the raft thicknesses of 0.75 m, 1 m, 1.5 m, and 2 m the maximum values of the raft twist are 0.93 x 10^{-5} (1/m), 0.61 x 10^{-5} (1/m), 0.27 x 10^{-5} (1/m), and 0.12 x 10^{-5} (1/m), respectively.

For the different raft thicknesses, the maximum raft twist is observed when the tunnel face is directly beneath the raft centerline. As the raft thickness increases, the permanent twist deformation value decreases and becomes almost zero at d = 2.00 m, which indicates that that raft stiffness plays a significant role in the twist deformation of the raft.

4.4 Effect of raft weight (w)

The effect of the raft weight is studied by comparing the results of two raft thicknesses of 1 m and 2 m while neglecting the raft weight (weightless raft). The effect of raft weight on the raft twist deformation is negligible, as shown in Figure 8. The raft twist deformation is primarily dependent on the differential settlement of the corners. As the raft weight is a uniform load, it will not have a significant influence on the differential settlement values; accordingly, the raft twist deformation is unaffected

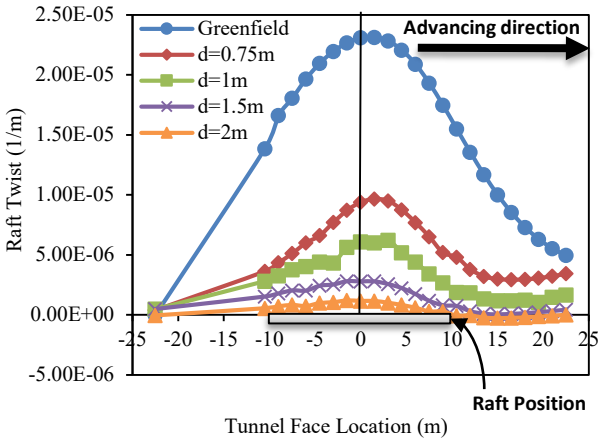

Figure 7. Effect of raft thickness (d) on raft twist (Θ).

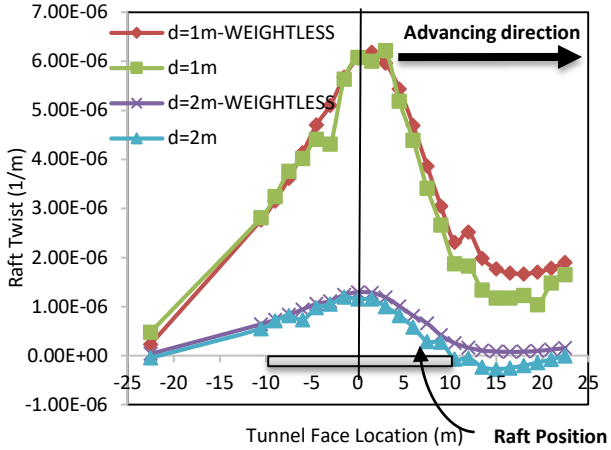

Figure 8. Influence of raft weight (w) on raft twist (Θ).

5 CONCLUSIONS

In this study, the finite element numerical simulation succeeded in simulating the complicated TBM shield tunneling method. The model output has been validated through a comparison with the field measurements of the settlement trough recorded during the construction of the Second Heinenoord tunnel in the Netherlands (1998). Moreover, the 3D modeling allows simulating both the tunnel and the raft on the ground surface, which helps in studying the complex interaction between the tunnel and the raft with different geometrical configurations.

The raft twist deformation is calculated during the tunnel advancement process, and the 3D nature of the raft twist phenomenon has been captured using the 3D numerical modeling. A sensitivity analysis is conducted to evaluate the effect of different geometrical and structural parameters. The raft twist deformation is significantly affected by the tunnel cover (Z), the skew angle between raft and tunnel (i), and the raft thickness (d). However, the effect of raft weight (w) is negligible. If the existing raft and

the new tunnel are perpendicular to each other, a temporary peak twist deformation is expected when the tunnel is directly beneath the raft centerline, but this twist deformation tends to vanish when the tunnel face crosses the raft edge. On the other hand, a permanent value of twist deformation is observed if there is a skew angle between the raft and the tunnel. When changing the raft thickness, the induced permanent twist behavior tends to vanish when the raft thickness equals 2 m.

6 REFERENCES

Bernat, S., Cambou, B., 1998. Soil-structure interaction in shield tunneling in soft soil. *Journal of Computational Geotechnique*, 22: 221–242.

Burd, H.J., Houlsby, G.T., Augarde, C.E., Liu, G., 2000. Modeling tunneling-induced settlement of masonry buildings. In: *Proceedings of the ICE, Geotechnical Engineering*, 143(1): 17–29.

Dimmock, P.S., Mair, R.J., 2008. Effect of building stiffness on tunneling-induced ground movement. *Journal of Tunneling and Underground Space Technology,* 23: 438–450.

Elmouchi, A., Hassan, A.M., Amer, M.I., 2017. Effect of using TBM tunneling in granular soils on the performance of an existing raft foundation. GeoMEast 2017 International Congress and Exhibition "Sustainable Civil Infrastructures: Innovative Infrastructure Geotechnology," Sharm El Sheikh, Egypt.

Elmouchi, A., Hassan, A.M., and Amer, M.I., 2018. Performance of an Existing Raft Foundation Rested on Granular Soils Due to TBM Tunneling Process, *Arabian Journal of Geosciences*, 11:108.

Franzius, J.N., Potts, D.M., Burland, J.B., 2006. Twist Behavior of buildings due to tunnel induced ground movement. Geotechnical Aspects of Underground Construction in Soft Ground – Proceedings of the 5th International Conference of TC28 of the ISSMGE Amsterdam – The Netherlands.

Keshuan, M., Lieyun, D., 2008. A full 3-D finite element analysis of the prediction between river-crossing tunneling and adjacent building. In: Proceedings of World Tunnel Congress on Underground Facilities for Better Environment and Safety, India.

Liu, H.Y., Small, J.C., Carter, J.P., 2008. Full 3D modeling for effects of tunneling on existing support systems in the Sydney region. *Journal of Tunneling and Underground Space Technology,* 23: 399–420.

Moller, S., 2006. Tunnel induced settlements and structural forces in lining: *Ph.D. Dissertation*, Department of Geotechnical Engineering, University of Stuttgart, Stuttgart.

Mroueh, H., and Shahrour, I. 2003. A full 3-D finite element analysis of tunneling–adjacent structures interaction. *Computers and Geotechnics,* 30:245–253.

Peck, R.B., 1969. Deep excavation and tunneling in soft ground. In: Proceedings of 7th International Conference on Soil Mechanic Foundation Engineering, Mexico, State-of-the-Art Volume, pp. 225–290.

Pickhavar, J.A., Burd, H.J., Houlsby, G.T., 2010. An equivalent beam method to model masonry building in 3D finite element analysis. *Journal of Computational Geotechnique*, 88: 1049–1063.

Sagasta, C., 1987. Analysis of undrained soil deformation due to ground loss. *Geotechnique*, 37: 301–320.

Siddiqua S., Elmouchi, A., Hassan, A.M., and Amer, M.I., 2018. Comparison of 2D and 3D finite element models of tunneling in granular soil under existing raft foundation. 71st Canadian Geotechnical Conference (GeoEdmonton 2018), Edmonton, Canada.

Verruijt, A., Booker, J.R., 1996. Surface settlements due to deformation of tunnel in an elastic half plane. *Geotechnique,* 46: 753–757.